THE ROLE OF HFL1 IN LYSOSOMAL HOMEOSTASIS

by

Seth Lilavivat

A thesis submitted to the faculty of
The University of Utah
in partial fulfillment of the requirements for the degree of

Master of Science

Department of Biochemistry

The University of Utah

December 2013

The University of Utah Graduate School

STATEMENT OF THESIS APPROVAL

The thesis of **Seth Lilavivat**

has been approved by the following supervisory committee members:

Adam S. Frost	, Chair	**13-Sept-2013** Date Approved
Christopher P. Hill	, Member	**13-Sept-2013** Date Approved
Diane M. Ward	, Member	**16-Sept-2013** Date Approved

and by **Christopher P. Hill** , Chair/Dean of

the Department/College/School of **Biochemistry**

and by David B. Kieda, Dean of The Graduate School.

ABSTRACT

In eukaryotes, lysosomes are dynamic organelles that change their size and shape depending on environmental and biological conditions. An emerging paradigm in lysosome biology is that size and copy number are regulated by an equilibrium between continuous cycles of fusion and fission. We discovered a novel gene, SPAC30D11.06c, that encodes a lysosomal membrane protein. The gene was appropriately named HFL1 (Has Fused Lysosomes) because in the null mutant, perinuclear lysosomes fuse together into long tubules. In this work, we established biochemical conditions to solubilize and purify HFL1 from crude cell lysate and performed a co-immuniprecipitation of HFL1 to identify possible protein partners that might inform on HFL1 function. The results of this study demonstrate that HFL1 can be isolated and studied *in vitro* providing important tools for future studies exploring HFL1 function.

TABLE OF CONTENTS

LIST OF FIGURES

ACKNOWLEDGEMENTS

I express gratitude to my committee members, Adam Frost, Chris Hill, and Diane Ward, for their support, encouragement, and constructive criticism. My time as a student has been a process of learning as a scientist and growing as a person. I would like to particularly thank Adam Frost, who mentored me as a student for the work described here. I express gratitude to my former graduate student advisor from the Department of Chemistry, Ken Woycechowsky, who helped me successfully accomplish work that is not described here and molded me as a student. I thank my former committee members while I was in the Department of Chemistry, Jennifer Heemstra, Martin Horvath, Ryan Looper, and Dale Poulter, who were all constructive and encouraging during my foray in the Department of Chemistry.

I have a deep sense of gratitude for my first advisor Nicholas Hud, who inspired my love of Science. Nick was extremely generous in giving me the opportunity to work in his lab. I feel extremely fortunate that I had the opportunity to work on daunting yet fascinating questions, and this opportunity enabled me to see my own potential. I thank Nick for being a positive role model both in his work and personal life. He was enthusiastic, encouraging, and held the highest standard of character.

Most of all, I would like to thank my family for always supporting me and encouraging me to follow my dreams and give my best. I express gratitude to my caring girlfriend, Caitlin, who has supported me through much of my time as a graduate student.

CHAPTER 1

INTRODUCTION

1.1 Statement of Problem

In eukaryotes, lysosomes are hydrolytic, acidified organelles that break down food particles, failing organelles, and pathogens such as viruses and bacteria. These materials are broken down into chemical building blocks so they can be recycled to make new biomolecules. Substrates are delivered to lysosomes by late endosomes, phagosomes, and autophagosomes, depending on the specific biological molecules to be degraded and metabolic needs of the cell. Therefore, the flux of membranes and enzymes trafficking through the lysosomal pathway varies and is closely tied to cell metabolism, nutrient availability (Poüs and Codogno, 2011), and times when cells must alter their structure or function (Guan et al., 2013). How lysosomes maintain optimal function is currently an exciting area of research because misregulation of lysosome function is the cause of many human diseases.

The ability of lysosomes to change size and copy number is critical for regulating osmolarity, organelle inheritance, and responding to nutrient availability (Bone et al., 1998; Storrie and Desjardins, 1996; Weisman, 2003). Size and copy number are controlled by the relative rates of organelle fusion and fission (Baars et al., 2007), but little is known about how these rates are regulated. This study focuses on the discovery

of a new factor that could be involved in lysosome homeostasis. Here, we describe how the factor was identified, the phenotype of the null mutant, and hypothesize how it affects lysosomal homeostasis. This study provides preliminary data needed to guide research aimed at revealing how lysosome fusion and fission events are controlled.

1.2 The Lysosomal Fusion Pathway

The dynamics of lysosomes has been studied most extensively in the budding yeast *Saccharomyces cerevisiae* because their large vacuoles are convenient for microscopy and their genetics are easy to manipulate (Weisman, 2003; Wickner, 2010). Homotypic vacuole fusion is well characterized and mostly understood, in large part because of the ability to examine and reconstitute fusion *in vitro* (Haas et al., 1994).

Fusion can be divided into three stages of sequential reactions: priming, docking, and fusing (Figure 1.1) (Wickner, 2010). SNAREs (soluble *N*-ethylmaleimide-sensitive factor [NSF] attachment receptors) are small α-helical forming proteins anchored onto the surface of lipid membranes (Fukuda et al., 2000). On yeast vacuoles, they form a tight four-helix bundle in a *cis*-complex with the protein Sec17p. During priming, SNAREs are released from their *cis*-SNARE complexes in an ATP-dependent manner (Mayer et al., 1996; Ungermann et al., 1999).

Docking occurs in two substages: (1) tethering and (2) the formation of *trans*-SNARE complexes. Tethering begins with the activation of a small Rab GTPase, Rab7 (Ypt7 in yeast). Rab proteins play a central role in membrane fusion events in the endolysosomal pathway, specifically by supporting endosome to lysosome fusion (Wang et al., 2011). Rabs are activated by upstream guanine nucleotide exchange factors (GEFs) that convert the Rab's GDP bound state to GTP bound. This exchange results in a

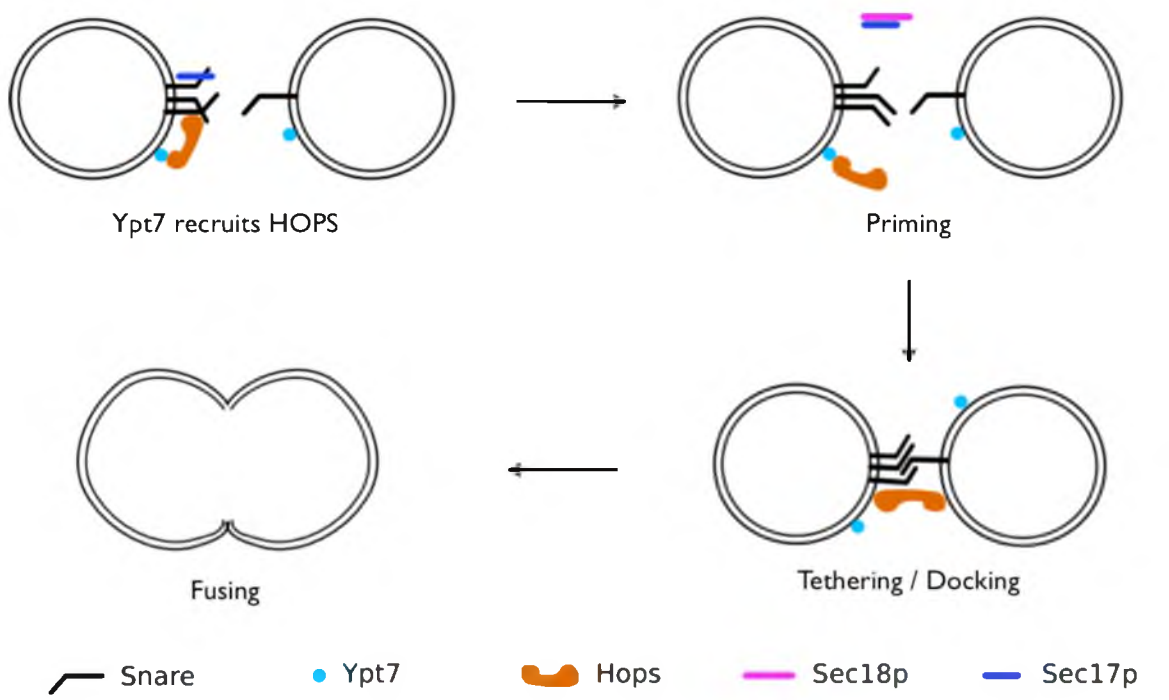

Figure 1.1 Simplified model of yeast homotypic vacuole fusion

conformational change that triggers the Rab to act on downstream effectors, such as recruiting proteins or activating other Rabs. Conversion of Ypt7-GDP to Ypt7-GTP is promoted by a subunit of the homotypic protein sorting (HOPS) complex. HOPS binds Ypt7-GTP and serves as a bridge and "tethers" two apposing vacuole membranes (Seals et al., 2000). Completion of docking results from the formation of a *trans*-SNARE complex in which three SNARE proteins from one membrane bind one SNARE from the opposite membrane as a four-helix bundle. This results in a stable association, although membrane fusion requires many other proteins and factors (Eitzen et al., 2001, 2002; Peters and Mayer, 1998; Strasser et al., 2011; Wang et al., 2003).

The precise events that take place during fusion are difficult to prove and heavily debated in the literature. One reason is that the conditions of *in vitro* reconstitution reactions can alter the requirements needed for membrane fusion. While SNAREs are

sufficient to drive fusion in certain *in vitro* reactions, it is generally accepted that membrane fusion between two lysosomes requires additional factors that destabilize apposing lipid membranes. For example, there is evidence that the polymerization of actin may play a role in destabilizing the lysosomal membrane at the point of fusion (Eitzen et al., 2002). Another more recent example implicates the V_0 sector of the V-ATPase in partnering with SNAREs to drive membrane fusion, independent of the V_0 function for proton translocation (Strasser et al., 2011). Many more factors are evidenced as possible regulators of lysosomal fusion, and through the analysis of genetic interaction data, the list continues to grow.

1.3 The Lysosomal Fission Pathway

Many intracellular organelles divide by membrane fission, including but not limited to mitochondria (Hermann and Shaw, 1998), Golgi (Corda et al., 2002; Shorter and Warren, 2002), peroxisomes (Yan et al., 2005), and endosomes (van der Goot and Gruenberg, 2006). The vacuoles of budding yeast cells divide to generate new vacuoles for daughter cells and fragment into smaller vacuoles during hypertonic conditions, possibly to maintain cytosolic osmolarity (Bone et al., 1998). Dynamin-like family GTPases have been implicated vacuolar in fragmentation in budding yeast, but many questions remain unanswered (Michaillat et al., 2012; Peters et al., 2004). Dynamins are involved in myriad membrane scission events by acting to constrict membranes when polymerized (Schmid and Frolov, 2011). If vacuoles and lysosomes divide using mechanisms similar to that in other organelles, then Vps1 would be the most likely candidate as the primary fission factor.

Vacuole fission also requires the lipid phosphatidylinositol 3,5-bisphosphate ($PI(3,5)P_2$) (Cooke et al., 1998; Gary et al., 1998) and a proton gradient, which is maintained by the H^+-ATPase (Baars et al., 2007). One possibility is that the vacuolar proton gradient is needed for water or ion transport in order to extrude water during vacuole fission. The expulsion of water is typically required because in order for organelles to divide while maintaining a constant surface area of membranes and overall shape, the volume inside the organelles must be reduced. Another possibility is that the proton gradient could alter the physical properties of the membrane bilayer by influencing surface charge or topology. In addition to fission, Vps1 is also involved in regulating vacuole fusion through its interactions with SNAREs (Alpadi et al., 2013). Furthermore, the V_0 sector of the H^+-ATPase has been implicated in driving lipid mixing in the final stages of vacuolar fusion (Baars et al., 2007; Strasser et al., 2011). The fact that Vps1 and V_0 regulate both fusion and fission suggests the existence of a homeostasis, but how homeostasis is regulated remains an open and important question.

1.4 Genetic Interactions of Vps1

A Genetic Interaction (GI) measures the functional relationship between two genes. GIs can be studied on a genome-scale using technologies such as Synthetic Genetic Array (SGA) analysis, a high-throughput technique used to systematically create double mutants on a large scale and then quantify their relative fitness. When a double mutant has a fitness that is significantly higher than expected from the product of the fitness of the individual mutants, the two deleted genes are considered to have a positive GI. A GI is considered to be negative when the double mutant shows a significantly lower than expected fitness, and in the severe case, the GI is lethal. In general, a positive

GI suggests that the two genes share pathways, whereas genes that have a negative GI are likely to exist on different pathways. Another metric used for quantifying the relationship between two genes is their correlation, which is expressed as the correlation coefficient between their genetic interactions with a common set of genes. A given gene has a correlation of 1.0 with itself, whereas the genetic correlation between two genes that are completely independent with each other is 0.0.

The ability to quantify genetic interactions on a genome-scale has been useful for discovering new genes and organizing genes into pathways. Recently, Frost et al. created a GI map that covered approximately 40% of the nonessential *S. pombe* genome in order to compare GIs in *S. pombe* with those in *S. cerevisiae* (Frost et al., 2012). This comparison was used to explore how genes may have been repurposed over the course of their evolutionary divergence, leading to the discovery of new functions for several proteins that are relevant for understanding mammalian cell biology. To gain insight into the mechanism of Vps1 during lysosome fusion and fission, we analyzed its GIs using the *S. pombe* data set (Figure 1.2). Vps1 shows strong genetic correlation (approximately 0.6) with apl3 and aps3, subunits of the AP-3 and AP-2 adaptor complexes, respectively. The AP-3 adaptor complex is involved in the budding of vesicles from the Golgi (Cowles et al., 1997), whereas the AP-2 adaptor complex is involved in clathrin-coated mediated endocytosis (Cremona and De Camilli, 1997). This would suggest that the function of Vps1 cooperates with membrane fission machinery, but is not limited to one membrane or organelle. Interestingly, Vps1 is synthetic lethal with the gene SPAC30D11.06c, a previously uncharacterized transmembrane protein. SPAC30D11.06c shows both positive GIs and correlation with components of endolysosomal system such as ESCRT III

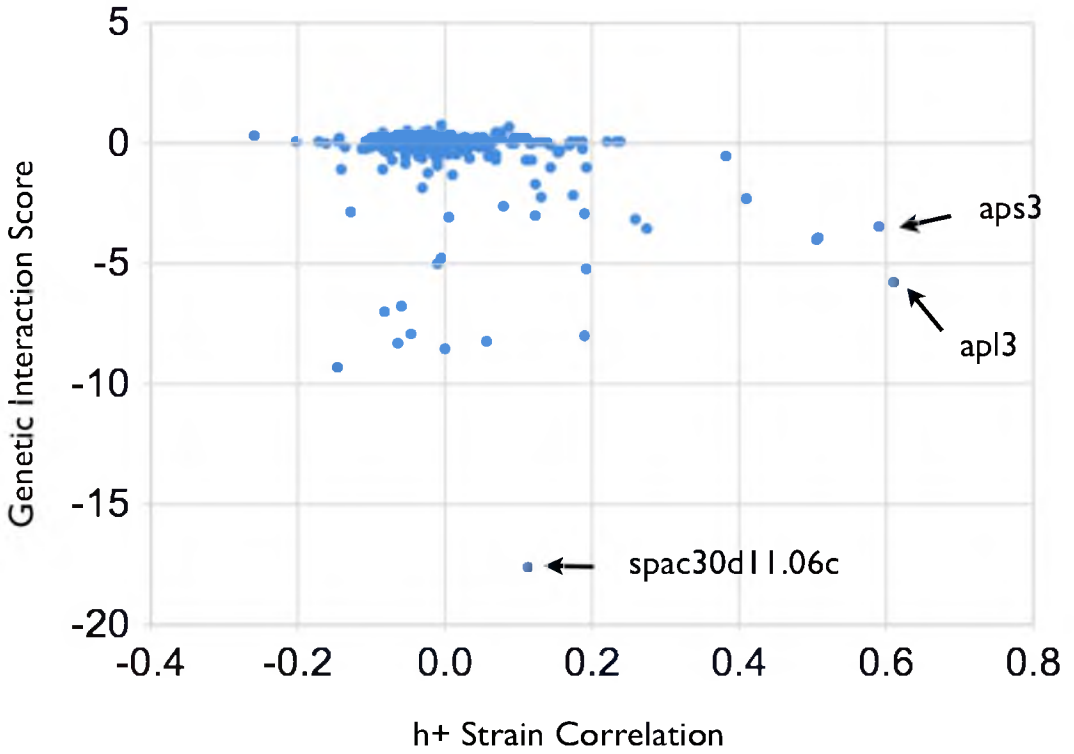

Figure 1.2 Genetic interaction profile of Vps1 in *S. pombe*. Arrows highlight aps3 and apl3, which have a strong positive correlation coefficient with vps1 and spac30d11.06c, which is synthetic lethal with vps1.

proteins (Vps20 and Vps60), endosomal trafficking machinery (Snx41 and Bro1), and regulators of lysosomal homeostasis (Lvs1) (Figure 1.3).

The synthetic lethality between Vps1 and SPAC30D11.06c supports the hypothesis that the two genes have parallel pathways but operate on a similar function. Synthetic lethal GIs are relatively rare, but their analysis provides a powerful tool for understanding genetic pathways and thus have been extensively studied in *Saccharomyces cerevisiae* (Ma et al., 2008). In general, the majority of synthetic lethal GIs occur when two parallel pathways are connected by a similar or overlapping function. While deleting one gene often impairs a cellular function, another pathway may

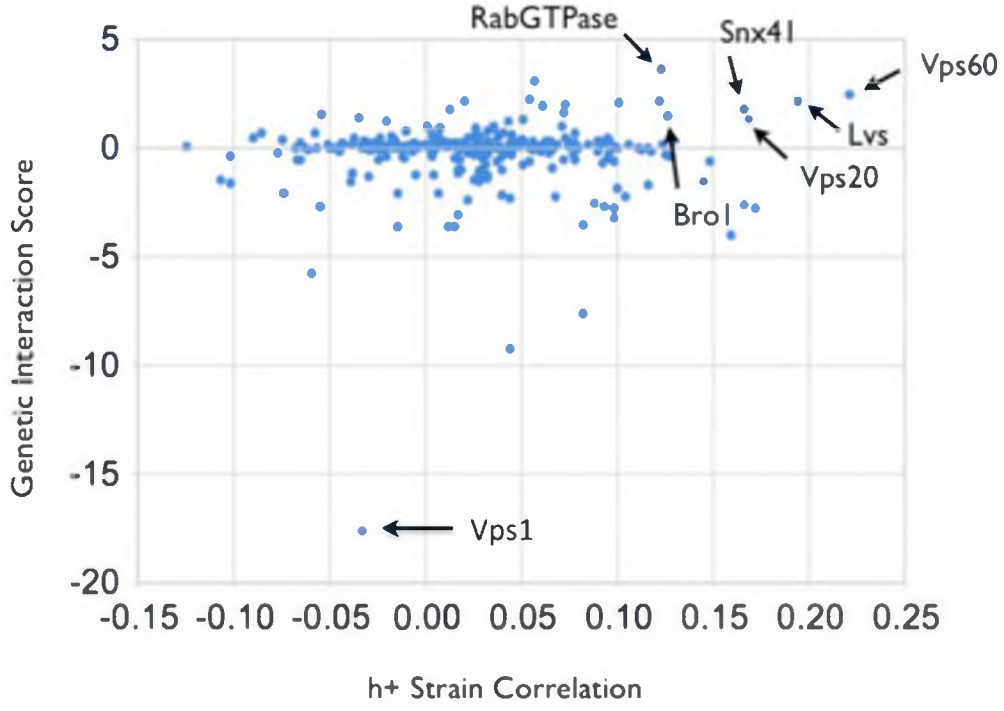

Figure 1.3 Genetic interaction profile of SPAC30D11.06c in *S. pombe*. Arrows highlight some of the genes involved in endosome and lysosome trafficking that are both positively correlated and have positive GI scores with spac30d11.06c

compensate to keep the cell viable, in which impeding both pathways is lethal. For example, the null mutant of SAC1, a gene that encodes a PI_4P phosphatase, results in nonlethal defects in endocytosis. A screen of genes that were lethal in a sac1Δ background led to the discovery that SAC1 was synthetic lethal with genes responsible for vacuolar and endosomal trafficking, such as the PI 3-kinase VPS34 (Tahirovic et al., 2005). This finding was important evidence that implicated the role of Sac1 in regulating intracellular PI_4P and contributed to the understanding of how phosphoinositides control membrane trafficking.

1.5 "Has Fused Lysosomes" (HFL1)

To determine the role that SPAC30D11.06c plays in cell function, its localization was examined by replacing the WT gene with one that expressed YFP fused to its C terminus. Microscopy revealed that SPAC30D11.06c is localized to the lysosomal membrane, suggesting it functions at the lysosome (A. Frost, unpublished data). To examine the morphology of lysosomes in ΔSPAC30D11.06c mutants, cells were treated with the dye FM4-64, which is incorporated into the plasma membrane and traffics to the lysosomes where it accumulates. Wild-type *S. pombe* have 10–30 small lysosomes that range from ~0.8 to ~1.2 microns in diameter, many localized to the perinuclear region of the cell. Deletion of SPAC30D11.06c in *S. pombe* reveals a striking phenotype—the lysosomes are fused together into elongated tubes (Figure 1.4) and in many cases appear to wrap around the nucleus. Images of live cells captured over 20 minutes indicate that the aberrant lysosomes are still capable of fusion and fission (Figure 1.4). Staining cells with the dye CDCFDA and expressing the fusion protein Ub-GFP-CPS, both of which accumulate in the lumen of lysosomes, confirmed the identity of the tubular structures as lysosomes (A. Frost, unpublished data). The morphology was further examined by Electron Microscopy of cells that were negatively stained and sectioned (Figure 1.5). These images reveal that the aberrant lysosomes are completely fused into narrow hollow tubes. Due to its unusual phenotype, SPAC30D11.06c was termed HFL1 for "has fused lysosomes." Elongated and tubular lysosomal membranes have been previously reported in Δatg8 cells treated with paraquat (Mikawa et al., 2010). Atg8 is a protein located at the autophagosome membrane and mediates lysosome to autophagsome fusion during autophagy. Atg8 also plays a role in vacuolar function apart from autophagy. Lysosomes

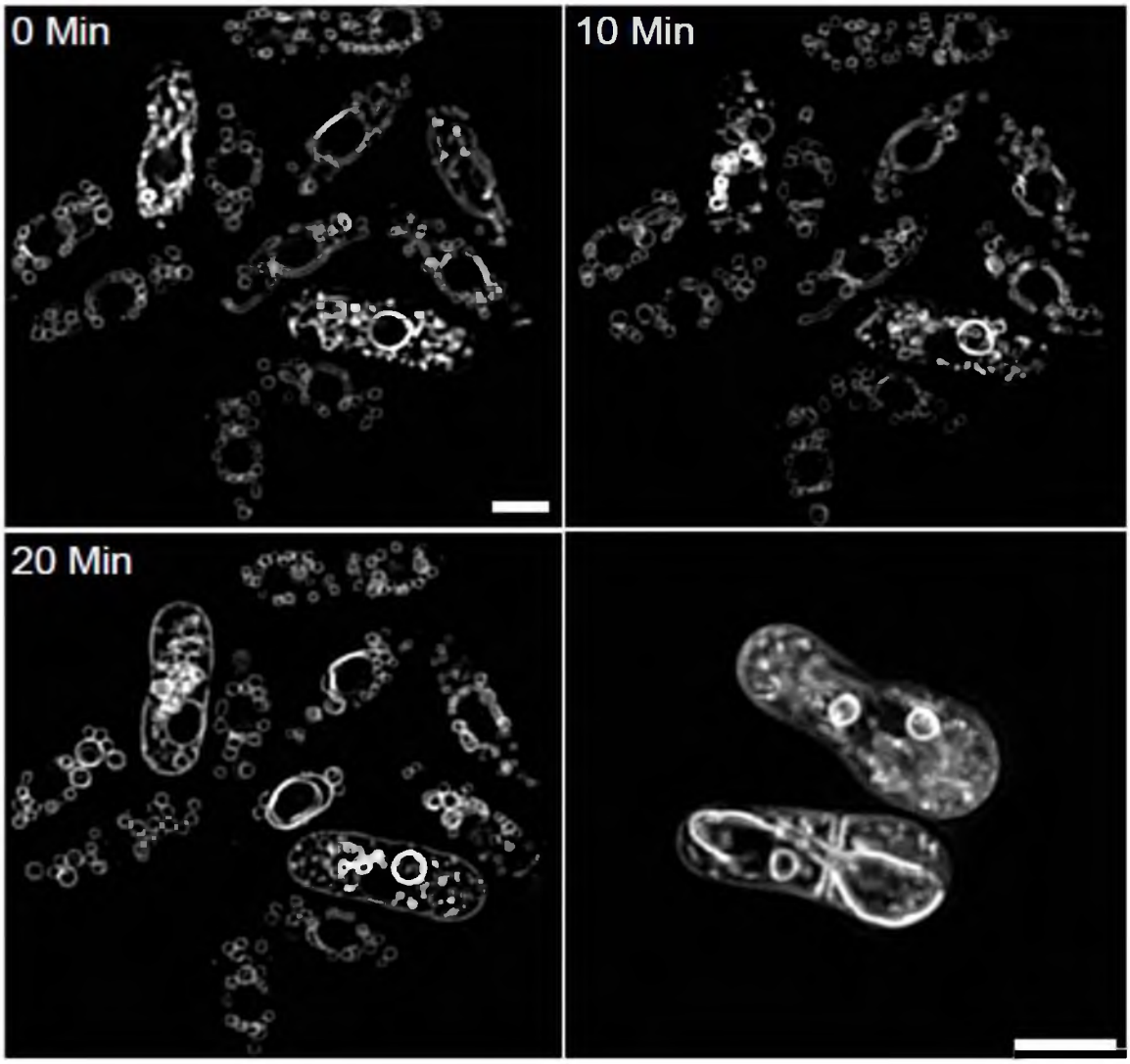

Figure 1.4 Phenotype of ΔHFL1 cells. Cells were treated were stained with FM4-64 and imaged over 20 minutes (A. Frost, unpublished data).

in Δatg8 *S. pombe* cells are similar to WT cells, but the addition of paraquat, which induces autophagy, causes a tubulation morphology similar to ΔHFL1. Interestingly, the unusual phenotype is rescued by the deletion of vps1, suggesting that Vps1 and Atg8 have antagonistic roles in vacuolar morphology, which is supported by a strong negative GI between the two genes in budding yeast. To the best of our knowledge the phenotype of ΔHFL1 is unique for cells under normal growth conditions.

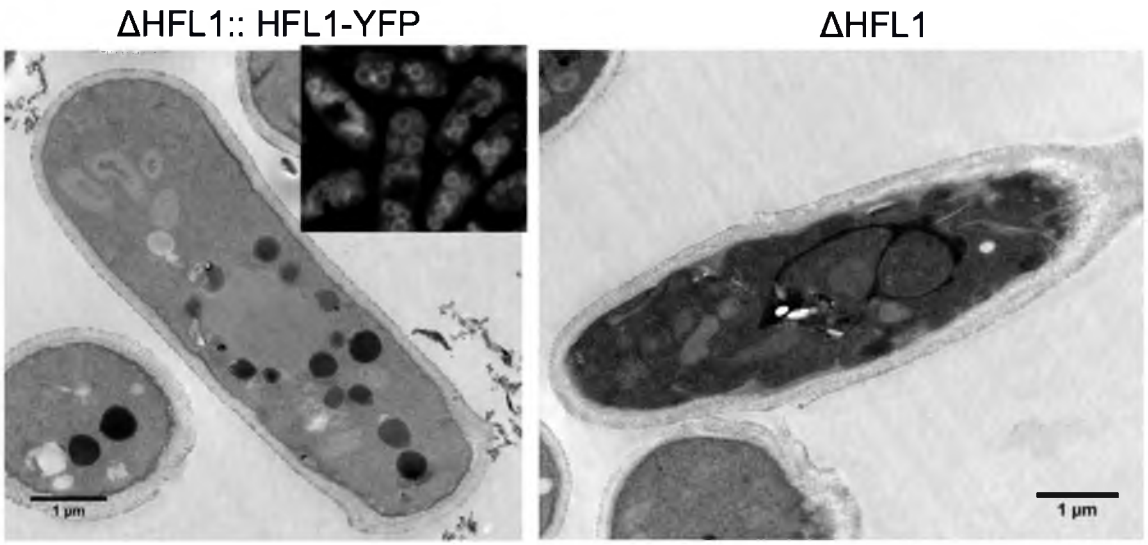

Figure 1.5 Transmission electron microscopy images of *S pombe* cells.
ΔHFL1::HFL1-YFP (left panel) and ΔHFL1 (right panel). The cells were fixed and sectioned as described previously (Wright, 2000). The inset in the left panel shows fluorescence microscopy images of ΔHFL1::HFL1-YFP, taken at the YFP channel.

1.6 Sequence Homology and Secondary Structure Prediction of HFL1

HFL1 encodes a 426 amino acid protein that has two distinct domains and shares close homology to its mammalian ortholog Transmembrane Protein 184b (Tmem184b). Tmem184b has not been characterized biochemically, and little is know about its function except that its regulation may play an important role in anaplastic thyroid cancer (Akaishi et al., 2007). In 11 anaplasitc thyroid cancer cell lines, Tmem34 (currently Tmem184b) was significantly down-regulated compared to normal thyroid cell lines. Additionally, transfection of Tmem184b into KTA2 cancer cells inhibited growth. Analysis of the primary sequence of HFL1 indicates that the N-terminus of the protein has approximately 250 amino acids that are predicted by the program TMHMM v. 2.0 to include 7 transmembrane helices (Figure 1.6). This transmembrane domain is homologous to the organic solute transport family (OST) of proteins, which are

Figure 1.6 Alignment between HFL1 and TMEM184B. The alignment was performed using ClustalW. The blue highlighted regions are predicted to be transmembrane helices using the program TMHMM v. 2.0.

responsible for transporting bile acids across the plasma membrane in cells that line the digestive system (Rao et al., 2008). It is unknown whether Tmem184b performs any transport function.

The C-terminal domain is predicted to contain no transmembrane segments and is predicted to be structurally disordered. Although it is rare for proteins to have large disordered regions, it is possible that disordered domains indicate regions where other proteins bind. The C-terminal domain is less conserved from fungi to humans, in that it is shorter and has a lower identity when compared to HFL1.

CHAPTER 2

THE BIOCHEMICAL CHARACTERIZATION OF HFL1

2.1 Methods

2.1.1 Liquid media and plates

The following media were used for growth and maintenance of *S. pombe*: YE5 (0.5% w/v yeast extract, 3.0% w/v glucose, 225 mg/L adenine, histidine, leucine, uracil, and lysine hydrochloride), SD -leu (0.5% w/v YNB without amino acids, 225 mg/L adenine, histidine, uracil, and lysine hydrochloride), EMM (3.2% w/v Sunrise Science EMM powder, 225 mg/L adenine, histidine, leucine, uracil, and lysine hydrochloride), and EMM -leu (3.2% w/v Sunrise Science EMM powder, 225 mg/L adenine, histidine, uracil, and lysine hydrochloride).

2.1.2 Growth and maintenance of *S. pombe* cultures

AF_JG_0001 and AF_JG_0029 were streaked onto SD -leu plates from glycerol stocks and incubated at 30 °C for approximately 72 hours or until the appearance of single colonies. Small liquid cultures (3–6 mL) of AF_JG_0001 were grown in EMM -leu media at 30 °C overnight or until the cell density reached an OD_{600} of approximately 1.0. Liquid cultures of AF_JG_0029 were grown in YE5. Large liquid cultures (50 mL–1L) of AF_JG_0001were grown in EMM-leu media shaking 180 rpm at 30 °C until the

cell density reached an OD_{600} of approximately 1.0–1.3. WT *S. pombe* strains were grown under the same conditions as AF_JG_0029.

2.1.3 Fluorescence microscopy of *S. pombe*

S. pombe cells were grown in 6 ml cultures at 30 °C until the OD_{600} reached approximately 0.8–1.0. Cells from 1 mL of culture were pelleted using a bench top mini centrifuge for approximately 5 seconds. Following centrifugation, the supernatant was discarded and the cell pellet was resuspended in approximately 10 µl of YE5 media. 1.5 µl of the cell suspension was placed on a glass slide and viewed at 100x.

2.1.4 Preparation of *S. pombe* cell lysates

S. pombe cells were harvested by centrifugation (5000 rpm for 10 minutes). For each 400 OD's of cells, 10 mL of 1x pombe Buffer (50mM HEPES pH 8.0, 100mM KCl, 1mM EDTA, and 15% (v/v) glycerol) were used to resuspend the cells. Then protease inhibitors PMSF, Pepstatin, Leupeptin, and Aprotinin were added to a final concentration of 1mM, 300mM, 8mM, and 0.3 µM, respectively. The cell suspension was frozen as small droplets by dripping the suspension slowly into liquid nitrogen and then stored at -80 °C. The frozen cell pellets were lysed by crushing them into a fine powder using a liquid nitrogen cooled mixer mill using the following protocol: 3 minutes of grinding at 10 RPM followed by 2 minutes of cooling, and the protocol was repeated for 15 cycles.

2.1.5 Western blotting of HFL1

Approximately 1 mL of crushed *S. pombe* powder was thawed on ice. A 10x solution of protease inhibitors (Roche Complete Mini) was added to a final concentration of 1x while the lysate was thawing. After thawing, an equal volume of 2x pombe Buffer

containing 4% digitonin (100mM HEPES pH 8.0, 100mM KCl, 2mM EDTA, 30% (v/v) glycerol, 4% digitonin) was added to the lysate. The cell slurry was then dispensed into 1.6 mL microcentrifuge tubes, filling at least 80% of the total volume, and then incubated at 4 °C for 1 hour while being gently rocked. The lysate was clarified of cell debris by table top centrifugation (13,000 rpm for 5 minutes). The supernatant was collected and the pellet was resuspended in 1x pombe buffer containing 8M Urea, and 6x SDS loading buffer was added to make a final concentration of 1x before storing the samples at -20 °C. 30 µl of each sample was separated on a 10% SDS-PAGE gel. The samples were transferred to nitrocellulose and blocked (using TBS, 5% milk) for 1 hour at room temperature. The nitrocellulose was incubated overnight at 4 °C with anti-GFP primary antibody (1:1000) in TBST, 5% milk, 0.02% NaN_3. After the membrane was rinsed three times (5 minutes in TBST), it was incubated with a secondary antibody conjugated to Alexa 647 (1:10,000) in TBST, 0.01% SDS for 1 hour at room temperature. The membrane was rinsed three times (15 minutes in TBST) before it was scanned and imaged at 700 nm.

2.1.6 Immunoprecipitation of HFL1

Approximately 10 mL of crushed *S. pombe* powder was thawed on ice to achieve a final volume of 5 mL. A 10x solution of protease inhibitors (Roche Complete Mini) was added to a final concentration of 1x while the lysate was thawing. After thawing, an equal volume of 2x pombe Buffer containing 4% digitonin (100mM HEPES pH 8.0, 100mM KCl, 2mM EDTA, 30% (v/v) glycerol, 4% digitonin) was added to the lysate. The lysate was incubated at 4 °C for 1 hour while gently rocking. The lysate was clarified of crude cell debris by centrifuging for 5 minutes at 15,000 rpm at 4 °C. 2 µl of Abcam

anti-GFP antibody was added to the supernatant and incubated at 4 °C for 1 hour while gently rocking. Then, 30 µl of an agarose bead slurry that binds to the primary antibody was incubated with the lysate overnight at 4 °C while gently rocking. The beads were collected after the overnight incubation by centrifuging the lysate at 3000 rpm for 1 minute. The beads were washed 5 times in 1 mL of 1x pombe buffer containing 2% digitonin. After the final wash step, the beads were finally resuspended in 100 µl of 1x pombe buffer containing 2% digitonin. 20 µl of the final bead-buffer mix was submitted for mass spectrometry analysis.

2.2 Results

2.2.1 Initial detection of HFL1

The first step of characterizing HFL1 was to detect the protein in crude cell lysate by Western blot. We chose to use the ΔHFL1::HFL1-YFP strain because YFP allowed the confirmation of HFL1 expression by microscopy and provided a convenient target for primary antibodies. When HFL1-YFP was expressed under the endogenous promoter, no protein was detected in the crude cell lysate, and low levels of protein corresponding to approximately 55 kDa were found in the crude pellet (Figure 2.1). We used a strain that expressed HFL1-YFP under the thiamine repressible nmt1 promoter in order to increase the yield. Despite over expressing HFL1-YFP, the majority of the protein remained in the pellet and showed considerable degradation. The Western blots only revealed N-terminal but not C-terminal degradation products because primary antibody (anti-GFP) binds to the YFP tag that is at the C-terminus of the target protein. Based on the presence of multiple fragments, it is most likely that the degradation is nonspecific and not the product of a biological function. It is not uncommon to experience difficulty isolating

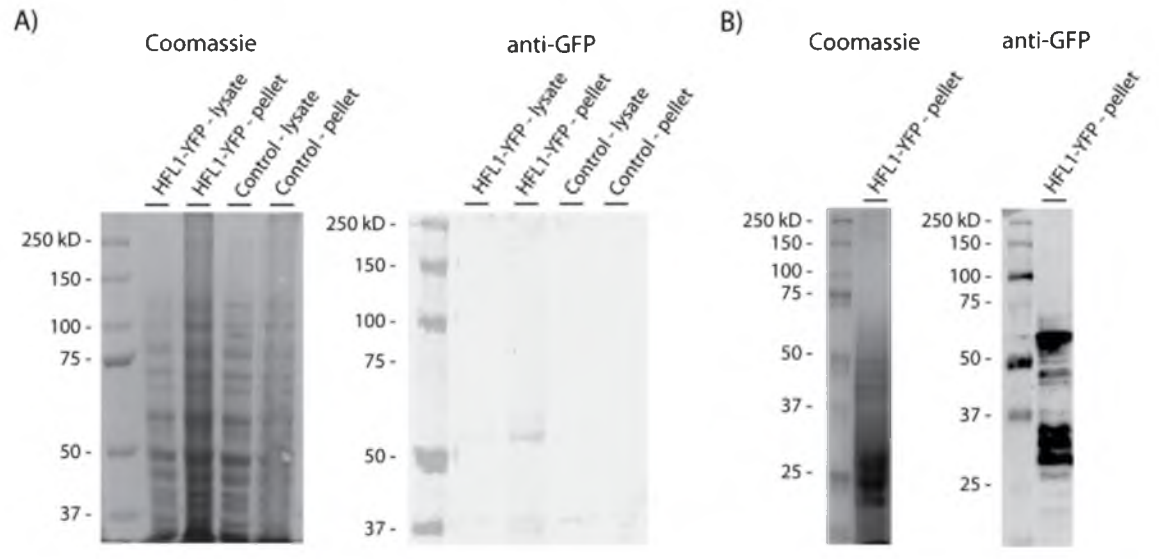

Figure 2.1 Initial isolation of HFL1-YFP from crude cell lysate. A) Coomassie and Western blot of cell lysates from *S. pombe* that endogenously expressed HFL1-YFP B) Coomassie and Western from *S. pombe* that over expressed HFL1-YFP using the nmt1 promotor

full-length proteins from lysosomes because they are filled with proteolytic enzymes. Considerable measures were taken to inhibit the activity of proteases during the preparation of cell lysate, including freezing the cell pellets in liquid nitrogen and lysing them under liquid nitrogen temperatures (see Methods). It is also possible that some of the protein degradation occurs prior to cell lysis.

2.2.2 Solubility of HFL1 using nondenaturing detergents

A major milestone towards the biochemical characterization of any protein is the ability to perform *in vitro* assays such as co-immunoprecipitations and pull-downs, which require identifying conditions where the protein is soluble. The hydrophobicity of membrane proteins can offer challenges when trying to utilize the proteins for assays. We screened HFL1 with three nondenaturing detergents, digitonin, Triton X-100, and NP-40,

in efforts to solubilize HFL1 while attempting to preserve its native structure and potential binding interactions (Figure 2.2). We optimized the isolation protocol of HFL1 using digitonin because it outperformed the other detergents in our initial screen (Figure 2.3). Buffer containing 1% (w/v) digitonin resulted in approximately 50% enrichment of the protein in the soluble fraction (crude supernatant). In addition, optimizing the isolation protocol using digitonin resulted in a major protein fragment of 65–70 kDa in solubilized fractions (Figure 2.3). The Western blot in Figure 2.3 also indicates the presence of an approximately 80 kDa protein that corresponds to full-length HFL1-YFP (right panel Figure 2.3).

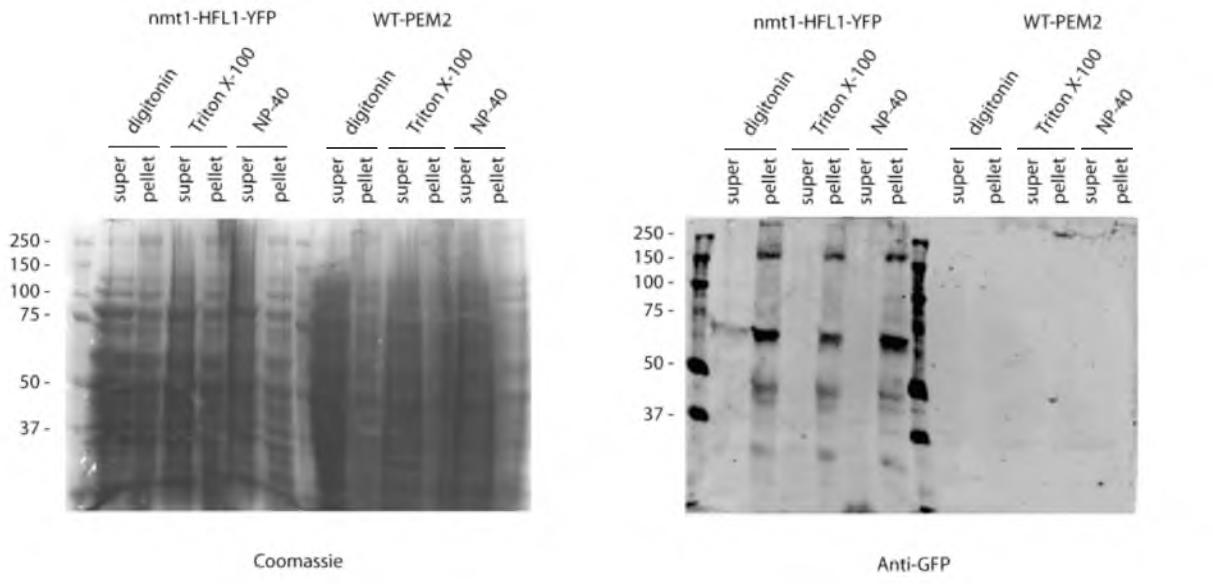

Figure 2.2 Examining the effect of three nondenaturing detergents on the solubility of HFL1-YFP. Crude cell lysates from *S. pombe* expressing HFL1-YFP were suspended in buffer containing 1% (w/v) digitonin, Triton X-100, and NP-40. After 5 minutes of table top centrifugation at 13,000 rpm, the lysate and pellet fractions were analyzed by Western blot to confirm the presence of HFL1-YFP.

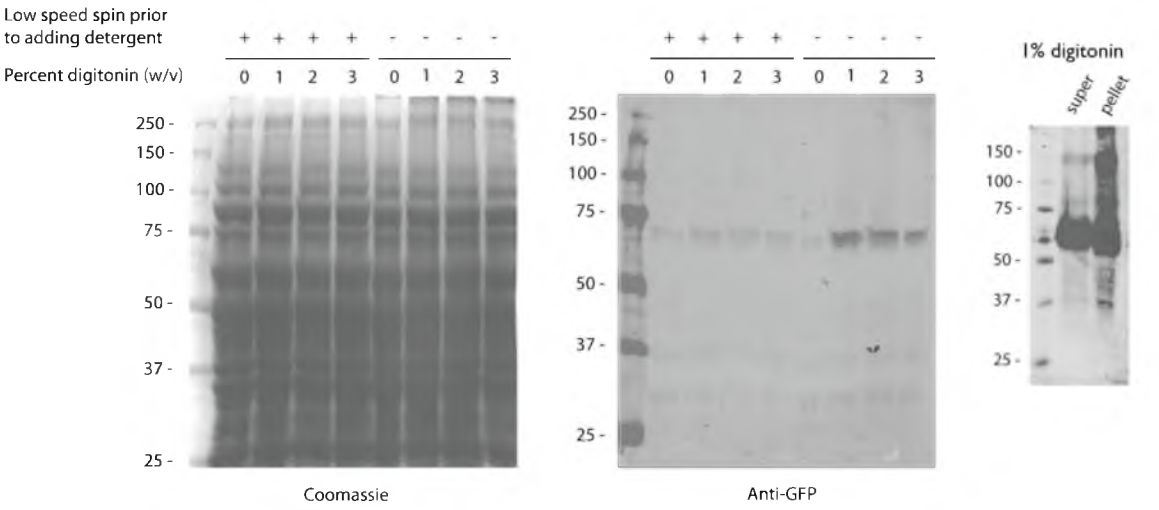

Figure 2.3 Solubilization of HFL1-YFP using digitonin. Crude cell lysates from *S. pombe* expressing HFL1-YFP were suspended in buffer containing 0–3% (w/v) digitonin, before and after a low speed spin (3000 rpm). After the addition of detergent, the mixture was spun on a benchtop centrifuged for 5 minutes at 13,000 rpm. The lysate and pellet fractions were analyzed by Western blot to confirm the presence of HFL1-YFP.

2.2.3 Co-immunoprecipitation of HFL1

After HFL1 was successfully solubilized, a co-immunoprecipitation (CO-IP) of HFL1 was used to identify potential binding partners. A serial two-step purification was used to enhance the purity of HFL1: step one was a Ni^{2+}-NTA affinity purification and step two was an anti-GFP affinity purification. The final step of the purification eluted agarose beads that bound our protein of interest and potentially proteins that bind to HFL1. We submitted 40 μl of the beads for protein identification by electrospray ionization (ESI) mass spec and analyzed 5 μl by Krypton stained gel and 5 μl by Western blot (Figure 2.4). Analysis of the Ni^{2+}-NTA purification elution reveals fragments (75, 90, 100, 140, and 150 kDa) that were not detected by Western blot, suggesting that these fragments are copurification products that do not associate with HFL1-YFP.

Interestingly, analysis of the agarose beads reveals two major bands (80 and >

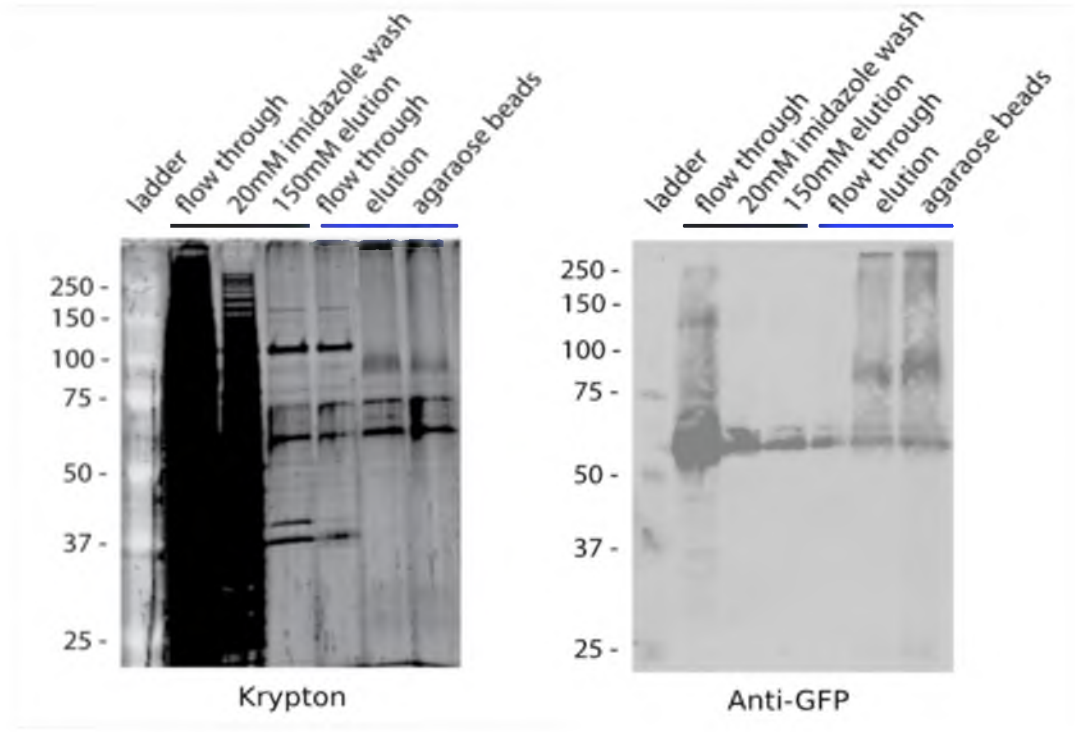

Figure 2.4 Tandem affinity purification CO-IP of HFL1-YFP. HFL1-YFP was purified by Ni^{2+}-NTA purification then immunoprecipitated. The fractions from the purification and the CO-IP were separated by SDS-PAGE and stained with Krypton (left panel) and analyzed by Western blot (right panel).

250 kDa) that were not present in the elution fraction of Ni^{2+}-NTA purified HFL1. Further analysis is needed to determine if these fragments are functional parters of HFL1 or merely artifacts of the CO-IP process, such as protein aggregates

The agarose beads used to for the CO-IP of HFL1-YFP were submitted to the core facilities for analysis by ESI mass spec. The mass spec data were used to query a database containing primary sequences of *S. pombe* proteins (Table 2.1). HFL1-YFP was the eighth most abundant protein suggesting high levels of contamination or poor protein purity (Table 2.1 row 8). Many of the proteins identified were ribosomal proteins, which often co-purify with membrane proteins since ribosomes are abundant mostly attached to

Table 2.1 Proteins from CO-IP of HFL1-YFP identified by ESI mass spec

gi|19112946	glyceraldehyde-3-phosphate dehydrogenase Tdh1 [Schizosaccharomyces pombe 972h
gi|1136783	elongation factor 1 alpha-A [Schizosaccharomyces pombe]
gi|1200144	pyruvate kinase [Schizosaccharomyces pombe]
gi|1749736	unnamed protein product [Schizosaccharomyces pombe]
gi|19113522	phosphoglycerate kinase Pgk1 (predicted) [Schizosaccharomyces pombe 972h-]
gi|19112695	enolase [Schizosaccharomyces pombe 972h-]
gi|19114264	homocysteine methyltransferase [Schizosaccharomyces pombe 972h-]
gi|19114123	DUF300 family protein [Schizosaccharomyces pombe 972h-]
gi|19075921	heat shock protein Ssa2 [Schizosaccharomyces pombe 972h-]
gi|19112372	adenosylhomocysteinase (predicted) [Schizosaccharomyces pombe 972h-]
gi|19112358	histone H4 h4.2 [Schizosaccharomyces pombe 972h-]
gi|19113555	40S ribosomal protein S3 [Schizosaccharomyces pombe 972h-]
gi|1304269	actin [Schizosaccharomyces pombe]
gi|19113523	S-adenosylmethionine synthetase [Schizosaccharomyces pombe 972h-]
gi|19112529	40S ribosomal protein S14 [Schizosaccharomyces pombe 972h-]
gi|2275296	60S ribosomal protein L31 homolog [Schizosaccharomyces pombe]
gi|19075524	triosephosphate isomerase [Schizosaccharomyces pombe 972h-]
gi|19075723	Cu metalloregulatory transcription factor Cuf2 [Schizosaccharomyces pombe 972h-]
gi|19114076	gamma-glutamyl phosphate reductase Pro1 (predicted) [Schizosaccharomyces pombe]
gi|1749428	unnamed protein product [Schizosaccharomyces pombe]
gi|19115272	P-type proton ATPase Pma1 [Schizosaccharomyces pombe 972h-]
gi|19075512	40S ribosomal protein S17 [Schizosaccharomyces pombe 972h-]
gi|623613	heat shock protein 90 [Schizosaccharomyces pombe]
gi|19113298	40S ribosomal protein S18 [Schizosaccharomyces pombe 972h-]
gi|122076	RecName: Full=Histone H3.3
gi|19114949	glycine hydroxymethyltransferase (predicted) [Schizosaccharomyces pombe 972h-]
gi|14277798	Chain A, Crystal Structure Of Inositol Polyphosphate 5-Phosphatase Domain (Ip
gi|563621	nmt2 [Schizosaccharomyces pombe]
gi|19114146	40S ribosomal protein S15a [Schizosaccharomyces pombe 972h-]
gi|2897739	ribosomal protein S9 [Schizosaccharomyces pombe]
gi|6474784	40s ribosomal protein RP10 [Schizosaccharomyces pombe]
gi|19112841	mitotic cohesin complex subunit Psm1 [Schizosaccharomyces pombe 972h-]
gi|19112446	60S ribosomal protein L26 [Schizosaccharomyces pombe 972h-]
gi|173405	histone H2B-alpha [Schizosaccharomyces pombe]
gi|19075701	nucleoside diphosphatase Ynd1 [Schizosaccharomyces pombe 972h-]
gi|3628750	ribosomal protein S16 homolog [Schizosaccharomyces pombe]
gi|19113072	conserved protein [Schizosaccharomyces pombe 972h-]
gi|2645173	sts5+ [Schizosaccharomyces pombe]
gi|19075744	alcohol dehydrogenase Adh1 [Schizosaccharomyces pombe 972h-]
gi|2641944	elongation factor 2 [Schizosaccharomyces pombe]
gi|19112602	chaperonin-containing T-complex gamma subunit Cct3 [Schizosaccharomyces pombe]
gi|398159	fructose 1,6-bisphosphate aldolase [Schizosaccharomyces pombe]
gi|19112949	Mago binding protein homolog [Schizosaccharomyces pombe 972h-]
gi|19112817	conserved fungal protein [Schizosaccharomyces pombe 972h-]
gi|19112441	sequence orphan [Schizosaccharomyces pombe 972h-]
gi|19114980	DNA polymerase zeta catalytic subunit Rev3 [Schizosaccharomyces pombe 972h-]
gi|19115492	GTPase Ypt2 [Schizosaccharomyces pombe 972h-]

HFL1-YFP was purified using a sequential Ni^{2+}-NTA / anti-GFP method. The proteins were identified using the software MASCOT and are listed in decending order according to their score.

the ER membrane. None of the proteins found in significant abundance are lysosomal membrane proteins or implicated in endolysosomal trafficking. Thus the CO-IP did not identify good candidates for proteins in a stoichiometric complex with HFL1-YFP.

The CO-IP was repeated in which a serial two-step purification was used as well as a single-step anti-GFP purification (Figure 2.5). Analysis of fractions using a Krypton stained gel suggests that the protein yield was lower in the second CO-IP experiment compared to the first. Western blot of purification fragments show large smears in the range of 25–50 kDa, suggesting a high level of degradation that was not present during the first CO-IP experiment. Agarose beads from the two-step purification and the single-step purification were submitted for analysis by ESI mass spec (Table 2.2 and Table 2.3).

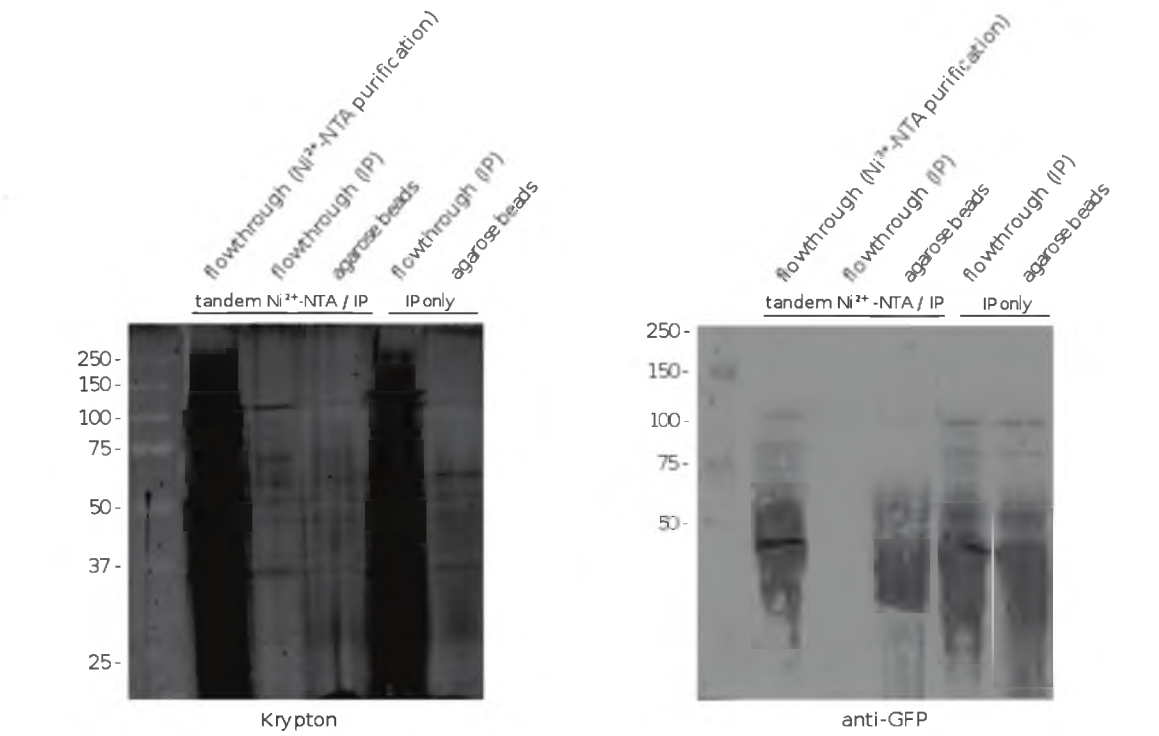

Figure 2.5 Tandem affinity purification CO-IP and CO-IP only of HFL1. HFL1-YFP was purified by Ni^{2+}-NTA purification then immunoprecipitated. In parallel, FL1-YFP was immunoprecipated without a Ni^{2+}-NTA purification step. The fractions from the purification and the CO-IP were separated by SDS-PAGE and stained with Krypton (left panel) and analyzed by Western blot (right panel).

Table 2.2 Proteins from CO-IP of HFL1-YFP identified by ESI mass spec

gi|19112946	glyceraldehyde-3-phosphate dehydrogenase Tdh1 [Schizosaccharomyces pombe 972h-]
gi|1136783	elongation factor 1 alpha-A [Schizosaccharomyces pombe]
gi|19114264	homocysteine methyltransferase [Schizosaccharomyces pombe 972h-]
gi|295442915	pyruvate decarboxylase (predicted) [Schizosaccharomyces pombe 972h-]
gi|19112695	enolase [Schizosaccharomyces pombe 972h-]
gi|19075921	heat shock protein Ssa2 [Schizosaccharomyces pombe 972h-]
gi|19114383	60S ribosomal protein L3 [Schizosaccharomyces pombe 972h-]
gi|19113434	thiazole biosynthetic enzyme [Schizosaccharomyces pombe 972h-]
gi|19112372	adenosylhomocysteinase (predicted) [Schizosaccharomyces pombe 972h-]
gi|19075744	alcohol dehydrogenase Adh1 [Schizosaccharomyces pombe 972h-]
gi|19114123	DUF300 family protein [Schizosaccharomyces pombe 972h-]
gi|19113522	phosphoglycerate kinase Pgk1 (predicted) [Schizosaccharomyces pombe 972h-]
gi|19113298	40S ribosomal protein S18 [Schizosaccharomyces pombe 972h-]
gi|1200144	pyruvate kinase [Schizosaccharomyces pombe]
gi|19113555	40S ribosomal protein S3 [Schizosaccharomyces pombe 972h-]
gi|1304269	actin [Schizosaccharomyces pombe]
gi|19115272	P-type proton ATPase Pma1 [Schizosaccharomyces pombe 972h-]
gi|19114949	glycine hydroxymethyltransferase (predicted) [Schizosaccharomyces pombe 972h-]
gi|19113523	S-adenosylmethionine synthetase [Schizosaccharomyces pombe 972h-]
gi|2992158	Moc2 RNA helicase [Schizosaccharomyces pombe]
gi|3628750	ribosomal protein S16 homolog [Schizosaccharomyces pombe]
gi|19112037	40S ribosomal protein S17 [Schizosaccharomyces pombe 972h-]
gi|2897739	ribosomal protein S9 [Schizosaccharomyces pombe]
gi|623613	heat shock protein 90 [Schizosaccharomyces pombe]
gi|19075935	40S ribosomal protein S2 [Schizosaccharomyces pombe 972h-]
gi|19114146	40S ribosomal protein S15a [Schizosaccharomyces pombe 972h-]
gi|19112529	40S ribosomal protein S14 [Schizosaccharomyces pombe 972h-]
gi|2641944	elongation factor 2 [Schizosaccharomyces pombe]
gi|3299814	ribosomal protein L28 homolog [Schizosaccharomyces pombe]
gi|312177	ribosomal protein L2 [Schizosaccharomyces pombe]
gi|1902882	ribosomal protein YL16 homolog [Schizosaccharomyces pombe]
gi|1813337	ribosomal protein S11 homolog [Schizosaccharomyces pombe]
gi|19114012	40S ribosomal protein S8 [Schizosaccharomyces pombe 972h-]
gi|173515	triose-phosphate-isomerase [Schizosaccharomyces pombe]
gi|3724352	ribosomal protein S4 [Schizosaccharomyces pombe]
gi|2274801	ribosomal protein L4 [Schizosaccharomyces pombe]
gi|1359468	heat shock cognate [Schizosaccharomyces pombe]
gi|19075193	60S ribosomal protein L35 [Schizosaccharomyces pombe 972h-]
gi|2760155	ribosomal protein L19 [Schizosaccharomyces pombe]
gi|67993614	60S ribosomal protein L18 [Schizosaccharomyces pombe 972h-]
gi|19075214	60S ribosomal protein L24 [Schizosaccharomyces pombe 972h-]
gi|2647410	ribosomal protein L18 [Schizosaccharomyces pombe]
gi|1749700	unnamed protein product [Schizosaccharomyces pombe]
gi|19114966	pho88 family protein [Schizosaccharomyces pombe 972h-]
gi|19114836	60S ribosomal protein L14 (predicted) [Schizosaccharomyces pombe 972h-]

HFL1-YFP was purified using a sequential Ni^{2+}-NTA / anti-GFP method. The proteins were identified using the software MASCOT and are listed in decending order according to their score.

Table 2.3 Proteins from CO-IP of HFL1-YFP identified by ESI mass spec

gi|19112946	glyceraldehyde-3-phosphate dehydrogenase Tdh1 [Schizosaccharomyces pombe 972h-]
gi|295442915	pyruvate decarboxylase (predicted) [Schizosaccharomyces pombe 972h-]
gi|1136783	elongation factor 1 alpha-A [Schizosaccharomyces pombe]
gi|19075529	urease accessory protein UREG (predicted) [Schizosaccharomyces pombe 972h-]
gi|19112372	adenosylhomocysteinase (predicted) [Schizosaccharomyces pombe 972h-]
gi|563621	nmt2 [Schizosaccharomyces pombe]
gi|19114949	glycine hydroxymethyltransferase (predicted) [Schizosaccharomyces pombe 972h-]
gi|19113298	40S ribosomal protein S18 [Schizosaccharomyces pombe 972h-]
gi|1304269	actin [Schizosaccharomyces pombe]
gi|1200144	pyruvate kinase [Schizosaccharomyces pombe]
gi|19114146	40S ribosomal protein S15a [Schizosaccharomyces pombe 972h-]
gi|19114383	60S ribosomal protein L3 [Schizosaccharomyces pombe 972h-]
gi|19114012	40S ribosomal protein S8 [Schizosaccharomyces pombe 972h-]
gi|19112529	40S ribosomal protein S14 [Schizosaccharomyces pombe 972h-]
gi|19075935	40S ribosomal protein S2 [Schizosaccharomyces pombe 972h-]
gi|19112037	40S ribosomal protein S17 [Schizosaccharomyces pombe 972h-]
gi|67993614	60S ribosomal protein L18 [Schizosaccharomyces pombe 972h-]
gi|19114123	DUF300 family protein [Schizosaccharomyces pombe 972h-]
gi|3628750	ribosomal protein S16 homolog [Schizosaccharomyces pombe]
gi|19113189	60S ribosomal protein L18 [Schizosaccharomyces pombe 972h-]
gi|1841308	ribosomal protein S16 homolog [Schizosaccharomyces pombe]
gi|312177	ribosomal protein L2 [Schizosaccharomyces pombe]
gi|19113555	40S ribosomal protein S3 [Schizosaccharomyces pombe 972h-]
gi|19114264	homocysteine methyltransferase [Schizosaccharomyces pombe 972h-]
gi|1229151	heat-shock protein [Schizosaccharomyces pombe]
gi|19112446	60S ribosomal protein L26 [Schizosaccharomyces pombe 972h-]
gi|19075193	60S ribosomal protein L35 [Schizosaccharomyces pombe 972h-]
gi|19112397	40S ribosomal protein S10 [Schizosaccharomyces pombe 972h-]
gi|19114589	40S ribosomal protein S7 (predicted) [Schizosaccharomyces pombe 972h-]
gi|2897739	ribosomal protein S9 [Schizosaccharomyces pombe]
gi|19075744	alcohol dehydrogenase Adh1 [Schizosaccharomyces pombe 972h-]
gi|19075214	60S ribosomal protein L24 [Schizosaccharomyces pombe 972h-]

HFL1-YFP was purified using a single-step anti-GFP affinity purification. The proteins were identified using the software MASCOT and are listed in decending order according to their score.

Results from the second two-step CO-IP (Table 2.2) showed poor protein purity and background contamination that is similar to the first CO-IP (Table 2.1). In the second CO-IP, HFL1 was the eleventh most abundant protein. Both CO-IP experiments showed abundant levels of proteins that have functions unrelated to lysosome homeostasis such as: glyceraldehyde-3-phosphate dehydrogenase Tdh1, elongation factor 1 alpha-A, heat shock protein Ssa2, pyruvate kinase, homocysteine methyltransferase, phosphoglycerate kinase Pgk1, and enolase.

2.3 Discussion

Our first attempts to isolate HFL1-YFP indicated significant degradation and the absence of full-length product. Solubilization with digitonin reduced degradation and revealed the presence of minor bands that correspond to full-length HFL1-YFP. There are two possible reasons that degradation was reduced. First, the addition of digitonin reduced the amount of proteases in the crude lysate and/or lowered protease activity. Secondly, the handling technique and preparation time may have improved after repeating the protocol several times.

The yield of HFL1-YFP was lower than expected when expressing the protein from the native HFL1 promoter, possibly due to nonspecific degradation. C-terminal degradation may destroy YFP and result in a loss of signal from anti-GFP antibodies. Future studies are needed to investigate the levels of N and C-terminal degradation, such as fusing an epitope tag to the N-terminus of HFL1. Even after the solubilization of HFL1-YFP with digitonin, at least 50% of the protein was lost in the crude pellet, probably because lysosomes can associate with subcellular membranes and pellet with cellular debris. Isolating lysosomal membranes from other cellular membranes might enrich soluble HFL1 in cell lysate.

The CO-IP experiment did not reveal any obvious functional partners of HFL1. It is possible that degradation and solubility were contributing factors that reduced the yield of bait protein, ultimately diminishing the sensitivity of the assay. In addition, MS indicated poor protein puritiy, increasing the rate of false positives and background contamination. Future CO-IP experiments should address obtaining a more pure sample of HFL1. In addition, several CO-IP experiments should be performed using different

antibodies as well as control experiments in order to validate the authenticity of any observed protein-protein interactions. For future experiments, it would be useful to create HFL1 fusion proteins using other epitope tags and vary the location (N or C-terminus) of the tag. An N-terminally tagged HFL1 could be used for both characterizing the degradation pattern and as a second CO-IP target.

CHAPTER 3

CONCLUSIONS AND FUTURE EXPERIMENTS

These studies show that HFL1 is a membrane protein of the lysosome and is possibly a novel regulator of lysosomal homeostasis. Deletion of HFL1 results in lysosome enlargement, but whether HFL1 acts as a fission factor or antagonizes fusion remains unanswered. If HFL1 promotes fission, then its synthetic lethality with Vps1 suggests that the two genes function on parallel pathways. Developing a model that explains their synthetic lethality is difficult because of the limited knowledge we have on both proteins. A broad explanation is that Vps1 has functions outside of lysosome homeostasis, and it is perhaps these functions that make cells intolerable to the simultaneous loss of HFL1. Another possibility is that both HFL1 and Vps1 are fission factors but operate on parallel or compensatory pathways. Hypothesizing a functional relationship between HFL1 and Vps1 is complicated by the fact that Vps1 regulates both lysosomal fusion and fission; thus, more work is needed before a mechanistic hypothesis can be developed. Future studies should investigate the colocalization for both of these proteins, in both mutants and WT cells, because understanding the localization of Vps1 in ΔHFL1 cells may provide insight as to how Vps1 rescues ΔHFL1 from lethality.

The phenotype of ΔHFL1 is striking, and it begs the question, why are the lysosomes tubular? One simple explanation is that deletion of HFL1 increases the rate of

fusion over fission, thus increasing the surface area of each lysosome. Then if the overall volume inside the lysosomes does not proportionally increase, they become elongated, much like the way a balloon would stretch if it were to enlarge in area without receiving more air. This model is logical but does not explain the wealth of empirical phenotypic data on mutants of fusion and fission factors. Consider the case in budding yeast when HOPS is over expressed. Vacuoles enlarge by an increase in the rate of fusion but maintain a round shape (Caplan et al., 2001; Poupon et al., 2003). In another example, the deletion of Lvs1—an *S. pombe* homologue of the mammalian fission factor Chs1/Lyst—results in lysosomes that are enlarged but not elongated or tubulated (A. Frost, unpublished data). Perhaps lysosomes have a mechanism for sequestering and extruding water in response to an increase or decrease in size, and this mechanism is impaired in ΔHFL1. Examining the biological function of lysosomes in ΔHFL1 with future experiments may provide insight into some of these questions. For example, pH-sensitive dyes or fusion tags could be used to determine lysosomal acidification, and following the protein markers through the endolysosomal pathway could determine if lysosomal proteins are sorted to their correct destination.

Although the work presented here did not arrive to conclusions about the mechanism and function of HFL1, it did identify appropriate conditions, challenges, and characterization needed for future biochemical studies. First, HFL1 is prone to degradation, either while isolating the protein from crude cell lysate or within the lysosome prior to cell lysis. Careful measures are necessary to reduce the amount of degradation such as using adequate protease inhibitors and lysing the cells under liquid nitrogen temperatures. Some of the methods described in this work require an overnight

incubation of crude lysate at 4 °C, and perhaps additional proteases should be added periodically during these long incubation periods. Second, HFL1 can be partially solubilized using 1% (w/v) digitonin, which may also reduce protease degradation. Approximately half of the expressed protein remains in the crude pellet after the addition of digitonin. Continued effort should be made towards improving the enrichment of HFL1 in soluble cell lysates, perhaps using methods such as sucrose gradient density fractionation. In addition, other nonionic detergents should be investigated for the solubilization of HFL1. Third, HFL1 has two distinct domains that are dissimilar from one another. The N-terminal domain is embedded in the membrane while the C-terminal domain is not and is predicted to be highly disordered based on its sequence. Future studies should be aimed at characterizing these domains independently. Basic questions regarding the functionality of each domain can be addressed by examining the phenotype of lysosomes when only one of the domains is deleted from HFL1.

The concept of lysosomal homeostasis is contemporary, and the field is still in its infancy. Discovering the mechanism of fission may be the greatest advancement to understanding lysosome dynamics. An important frontier goal of lysosome biology is to understand how the processes of fusion and fission are regulated. This work investigated a novel protein HFL1 that could play a central role in lysosome homeostasis.

APPENDIX

Table A.1 *S. pombe* strains used for this study

Name	Genotype	Source
AF_JG_0001	hfl1(exons)::NAT leu1-32:::P_{nmt1}-Hfl1-YFP-FLAG-HIS-Leu1	A. Frost
AF_JG_0029	hfl1(exons)::NAT leu1-32:::P_{hfl1}-Hfl1-YFP-FLAG-HIS-Leu1	A. Frost

REFERENCES

Akaishi, J., Onda, M., Okamoto, J., Miyamoto, S., Nagahama, M., Ito, K., Yoshida, A., and Shimizu, K. (2007). Down-regulation of an inhibitor of cell growth, transmembrane protein 34 (TMEM34), in anaplastic thyroid cancer. J. Cancer Res. Clin. Oncol. *133*, 213–218.

Alpadi, K., Kulkarni, A., Namjoshi, S., Srinivasan, S., Sippel, K.H., Ayscough, K., Zieger, M., Schmidt, A., Mayer, A., Evangelista, M., et al. (2013). Dynamin-SNARE interactions control trans-SNARE formation in intracellular membrane fusion. Nat. Commun. *4*, 1704.

Baars, T.L., Petri, S., Peters, C., and Mayer, A. (2007). Role of the V-ATPase in regulation of the vacuolar fission–fusion equilibrium. Mol. Biol. Cell *18*, 3873–3882.

Bone, N., Millar, J.B., Toda, T., and Armstrong, J. (1998). Regulated vacuole fusion and fission in Schizosaccharomyces pombe: an osmotic response dependent on MAP kinases. Curr. Biol. *8*, 135–144.

Caplan, S., Hartnell, L.M., Aguilar, R.C., Naslavsky, N., and Bonifacino, J.S. (2001). Human Vam6p promotes lysosome clustering and fusion in vivo. J. Cell Biol. *154*, 109–122.

Cooke, F.T., Dove, S.K., McEwen, R.K., Painter, G., Holmes, A.B., Hall, M.N., Michell, R.H., and Parker, P.J. (1998). The stress-activated phosphatidylinositol 3-phosphate 5-kinase Fab1p is essential for vacuole function in S. cerevisiae. Curr. Biol. *8*, 1219–1222.

Corda, D., Hidalgo Carcedo, C., Bonazzi, M., Luini, A., and Spanò, S. (2002). Molecular aspects of membrane fission in the secretory pathway. Cell. Mol. Life Sci. *59*, 1819–1832.

Cowles, C.R., Odorizzi, G., Payne, G.S., and Emr, S.D. (1997). The AP-3 adaptor complex is essential for cargo-selective transport to the yeast vacuole. Cell *91*, 109–118.

Cremona, O., and De Camilli, P. (1997). Synaptic vesicle endocytosis. Curr. Opin. Neurobiol. *7*, 323–330.

Eitzen, G., Thorngren, N., and Wickner, W. (2001). Rho1p and Cdc42p act after Ypt7p to regulate vacuole docking. Embo J. *20*, 5650–5656.

Eitzen, G., Wang, L., Thorngren, N., and Wickner, W. (2002). Remodeling of organelle-bound actin is required for yeast vacuole fusion. J. Cell Biol. *158*, 669–679.

Frost, A., Elgort, M.G., Brandman, O., Ives, C., Collins, S.R., Miller-Vedam, L., Weibezahn, J., Hein, M.Y., Poser, I., and Mann, M. (2012). Functional repurposing revealed by comparing *S. pombe* and *S. cerevisiae* genetic interactions. Cell *149*, 1339–1352.

Fukuda, R., McNew, J.A., Weber, T., Parlati, F., Engel, T., Nickel, W., Rothman, J.E., and Söllner, T.H. (2000). Functional architecture of an intracellular membrane t-SNARE. Nature *407*, 198–202.

Gary, J.D., Wurmser, A.E., Bonangelino, C.J., Weisman, L.S., and Emr, S.D. (1998). Fab1p is essential for PtdIns(3)P 5-kinase activity and the maintenance of vacuolar size and membrane homeostasis. J. Cell Biol. *143*, 65–79.

Guan, J.-L., Simon, A.K., Prescott, M., Menendez, J.A., Liu, F., Wang, F., Wang, C., Wolvetang, E., Vazquez-Martin, A., and Zhang, J. (2013). Autophagy in stem cells. Autophagy *9*, 830–849.

Haas, A., Conradt, B., and Wickner, W. (1994). G-protein ligands inhibit in vitro reactions of vacuole inheritance. J. Cell Biol. *126*, 87–97.

Hermann, G.J., and Shaw, J.M. (1998). Mitochondrial dynamics in yeast. Annu. Rev. Cell Dev. Biol. *14*, 265–303.

Ma, X., Tarone, A.M., and Li, W. (2008). Mapping genetically compensatory pathways from synthetic lethal interactions in yeast. Plos One *3*, e1922.

Mayer, A., Wickner, W., and Haas, A. (1996). Sec18p (NSF)-driven release of Sec17p (alpha-SNAP) can precede docking and fusion of yeast vacuoles. Cell *85*, 83–94.

Michaillat, L., Baars, T.L., and Mayer, A. (2012). Cell-free reconstitution of vacuole membrane fragmentation reveals regulation of vacuole size and number by TORC1. Mol. Biol. Cell *23*, 881–895.

Mikawa, T., Kanoh, J., and Ishikawa, F. (2010). Fission yeast Vps1 and Atg8 contribute to oxidative stress resistance. Genes Cells Devoted Mol. Cell. Mech.

Peters, C., and Mayer, A. (1998). Ca2+/calmodulin signals the completion of docking and triggers a late step of vacuole fusion. Nature *396*, 575–580.

Peters, C., Baars, T.L., Bühler, S., and Mayer, A. (2004). Mutual control of membrane fission and fusion proteins. Cell *119*, 667–678.

Poupon, V., Stewart, A., Gray, S.R., Piper, R.C., and Luzio, J.P. (2003). The role of mVps18p in clustering, fusion, and intracellular localization of late endocytic organelles. Mol. Biol. Cell *14*, 4015–4027.

Poüs, C., and Codogno, P. (2011). Lysosome positioning coordinates mTORC1 activity and autophagy. Nat. Cell Biol. *13*, 342–344.

Rao, A., Haywood, J., Craddock, A.L., Belinsky, M.G., Kruh, G.D., and Dawson, P.A. (2008). The organic solute transporter α-β, Ostα-Ostβ, is essential for intestinal bile acid transport and homeostasis. Proc. Natl. Acad. Sci. *105*, 3891–3896.

Schmid, S.L., and Frolov, V.A. (2011). Dynamin: functional design of a membrane fission catalyst. Annu. Rev. Cell Dev. Biol. *27*, 79–105.

Seals, D.F., Eitzen, G., Margolis, N., Wickner, W.T., and Price, A. (2000). A Ypt/Rab effector complex containing the Sec1 homolog Vps33p is required for homotypic vacuole fusion. Proc. Natl. Acad. Sci. *97*, 9402–9407.

Shorter, J., and Warren, G. (2002). Golgi architecture and inheritance. Annu. Rev. Cell Dev. Biol. *18*, 379–420.

Storrie, B., and Desjardins, M. (1996). The biogenesis of lysosomes: is it a kiss and run, continuous fusion and fission process? BioEssays. *18*, 895–903.

Strasser, B., Iwaszkiewicz, J., Michielin, O., and Mayer, A. (2011). The V-ATPase proteolipid cylinder promotes the lipid-mixing stage of SNARE-dependent fusion of yeast vacuoles. Embo J. *30*, 4126–4141.

Tahirovic, S., Schorr, M., and Mayinger, P. (2005). Regulation of Intracellular Phosphatidylinositol-4-Phosphate by the Sac1 Lipid Phosphatase. Traffic *6*, 116–130.

Ungermann, C., von Mollard, G.F., Jensen, O.N., Margolis, N., Stevens, T.H., and Wickner, W. (1999). Three v-SNAREs and two t-SNAREs, present in a pentameric cis-SNARE complex on isolated vacuoles, are essential for homotypic fusion. J. Cell Biol. *145*, 1435–1442.

van der Goot, F.G., and Gruenberg, J. (2006). Intra-endosomal membrane traffic. Trends Cell Biol. *16*, 514–521.

Wang, C.-W., Stromhaug, P.E., Kauffman, E.J., Weisman, L.S., and Klionsky, D.J. (2003). Yeast homotypic vacuole fusion requires the Ccz1–Mon1 complex during the tethering/docking stage. J. Cell Biol. *163*, 973–985.

Wang, T., Ming, Z., Xiaochun, W., and Hong, W. (2011). Rab7: role of its protein interaction cascades in endo-lysosomal traffic. Cell. Signal. *23*, 516–521.

Weisman, L.S. (2003). Yeast vacuole inheritance and dynamics. Annu. Rev. Genet. *37*, 435–460.

Wickner, W. (2010). Membrane fusion: five lipids, four SNAREs, three chaperones, two nucleotides, and a Rab, all dancing in a ring on yeast vacuoles. Annu. Rev. Cell Dev. Biol. *26*, 115–136.

Wright, R. (2000). Transmission electron microscopy of yeast. Microsc. Res. Tech. *51*, 496–510.

Yan, M., Rayapuram, N., and Subramani, S. (2005). The control of peroxisome number and size during division and proliferation. Curr. Opin. Cell Biol. *17*, 376–383.